Load-Independent Wireless Power Transfer System for Multiple Loads Over a Long Distance

Chenwen Cheng, Fei Lu, *Member, IEEE*, Zhe Zhou, Weiguo Li, *Member, IEEE*, Chong Zhu, Hua Zhang, *Member, IEEE*, Zhanfeng Deng, Xi Chen, *Senior Member, IEEE*, and Chunting Chris Mi, *Fellow, IEEE*

***Abstract*—In this paper, a novel long-distance wireless power transfer (WPT) system using repeater coils is proposed to provide power supplies for the driver circuits in high-voltage applications, such as flexible alternative current transmission systems. Different from most of the existing wireless repeater systems where the load is only connected to the last coil and the repeater coils function solely as power relays, in the proposed system, multiple loads are powered by the repeaters. The repeater coils transfer power not only to the subsequent coils but also to the loads connected to them. Dual coil design is proposed for the repeaters with which load-independent characteristics are obtained with a suitable design of coupling coefficients. As a result, the load power can be easily adjusted without affecting each other. Load current characteristics and system efficiency have been analyzed in detail. The power transfer capability of the proposed system is illustrated for different coil quality factors and coupling coefficients. An experimental setup with 10 loads has been built to validate the effectiveness of the proposed long-distance WPT system. The maximum reachable system efficiency is about 84%.**

***Index Terms*—Constant current characteristics, dual coil design, load independent, long distance, wireless power transfer (WPT).**

I. Introduction

WIRELESS power transfer (WPT) technology has attracted more and more attention in both the academia and industry [1]–[5]. Usually, the power transfer distance is limited by the coil dimension in the WPT system. This is because the coupling coefficient between the transmitting and receiving coils decreases dramatically with a larger distance, and consequently the efficiency and power will significantly drop [6].

Manuscript received August 7, 2018; revised October 17, 2018; accepted November 26, 2018. Date of publication December 12, 2018; date of current version June 10, 2019. This work was supported by Global Energy Interconnection Research Institute Co., Ltd., under Grant GEIRI-DL-71-17-011 (State Grid Sci & Tech project: Research on the Magnetic-Resonant Wireless Power Transfer Technology for the High-Voltage Converter Valve in FACTS). Recommended for publication by Associate Editor D. Qiu. *(Corresponding author: Chunting Chris Mi.)*

C. Cheng, F. Lu, C. Zhu, H. Zhang, and C. C. Mi are with the San Diego State University, San Diego, CA 92182 USA (e-mail: cheng.cwen@gmail.com; fei.lu@drexel.edu; chong.zhu@sdsu.edu; hua.zhang@drexel.edu; mi@ieee.org).

Z. Zhou, W. Li, and Z. Deng are with the State Key Laboratory of Advanced Power Transmission Technology (Global Energy Interconnection Research Institute), Changping District, Beijing 102211, China (e-mail: zhouzhe@geiri.sgcc.com.cn; lwgmb90549@sina.com; iphone21@sina.com).

X. Chen is with the Global Energy Interconnection Research Institute North America, San Jose, CA 95134 USA (e-mail: xi.chen@geirina.net).

Color versions of one or more of the figures in this paper are available online at http://ieeexplore.ieee.org.

Digital Object Identifier 10.1109/TPEL.2018.2886329

In order to obtain an efficient power transfer over a long distance, repeater coils were used [7], [8]. Moreover, the energy transfer path can be modified by adjusting the angles of the repeater coils [9]. In [10], it shows that the maximum efficiency will slightly shift away from the resonant frequency due to the cross coupling between nonadjacent coils. The influence of repeater coils on the system efficiency was analyzed in [11]. Lee *et al.* [12] pointed out that the use of a repeater coil can improve the stability of the system efficiency without resulting in the frequency splitting. The repeater coils can also be used as impedance matching circuits in case the coupling coefficient between the transmitting and receiving coils varies in time [13]. A tuning technique was proposed to improve the system performance against load variations in [14]. The wireless power repeater system has been applied to transfer energy wirelessly to power an online monitoring system [15].

However, only one load is present in these papers, which is connected to the last coil in the WPT repeater system. In some applications, however, more than one load needs to be powered. For example, in the flexible alternative current transmission systems (FACTS), a high-power rating converter is usually adopted to realize the high power operation. However, the power rating of the commercial power electronics switch like IGBT is not high enough, which limits the power rating of the converter. Moreover, the grid voltage is very high, which may exceed the voltage rating of the switches. Thus, multiple switches need to be connected in series to withstand the high voltage [16], [17]. The driver circuits are used to ensure the normal operation of the switches, which needs isolated power supplies because reference potentials of these switches are different. The WPT technology provides an ideal solution to provide multiple isolated power supplies because no direct contact is needed. The multiple driver circuits form multiple loads for the WPT system [18]. Thus, the WPT system transferring power to multiple loads deserves to be studied in detail.

In [19], a WPT system transferring power to multiple loads was proposed, where the loads were connected to all the repeater coils. However, if one load resistance changes, the power of other loads will also change. It means that the load power depends on each other and the system needs a complicated control method when used in practical applications. Thus, an independent load power control method needs to be studied.

In fact, load-independent constant current or constant voltage output characteristics for two-coil WPT system have been

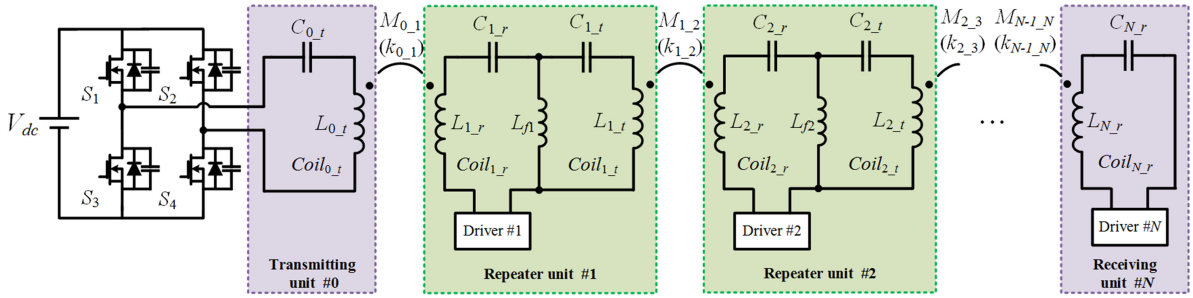

Fig. 1. Structure of the proposed WPT repeater system for gate drivers.

studied in [20]–[22]. With proper compensation topologies, either load-independent constant current or voltage output can be obtained. However, the independent constant output current or voltage characteristics are only studied in the two-coil WPT system while those in the WPT repeater system have not been studied yet.

In this paper, a novel WPT repeater system with multiple loads is proposed. In Section II, it will show that constant load currents with suitable coil design and compensation topologies can be obtained. The system's power transfer capability including the load current characteristics and system efficiencies are also analyzed when considering the parasitic resistances. Experimental results are given to validate the effectiveness of the proposed WPT repeater system.

II. Modeling of the Proposed WPT Repeater System

Fig. 1 shows the structure of the proposed WPT repeater system for gate driver circuits in FACTS. There are $(N+1)$ units in the system, which can be divided into three categories. Unit #0 is the transmitting unit, unit #*N* is the final receiving unit, and all the other units, from #1 to #$(N-1)$, are the repeater units. There are two coils in each repeater unit, where the first coil is used to receive power from the previous unit and the second one transfers power to the next unit. *L* is the self-inductance of the corresponding coil and *C* is the compensation capacitance. The number in the subscript of the *coil*, *L* and *C* indicates the unit number and the letter indicates whether it receives or transmits power. For example, $coil_{1\_r}$ is the receiving coil in unit #1 while $coil_{1\_t}$ is the transmitting coil in unit #1. Since the coil in unit #0 only transfers power to the next unit and the coil in unit #*N* only receives power from the previous unit, they are noted as $coil_{0\_t}$ and $coil_{N\_r}$, respectively. L_{f1}, L_{f2}, etc., are the auxiliary inductors in every repeater unit. $M_{0\_1}, M_{1\_2}, \ldots, M_{N-1\_N}$ are the mutual inductances between $coil_{0\_t}$ and $coil_{1\_r}$, $coil_{1\_t}$ and $coil_{2\_r}, \ldots, coil_{N-1\_t}$ and $coil_{N\_r}$, respectively. Their corresponding coupling coefficients $k_{0\_2}, k_{1\_2}, k_{2\_3}, \ldots, k_{N-1\_N}$ are defined as

$$k_{n\_n+1} = \frac{M_{n\_n+1}}{\sqrt{L_{n\_t} \cdot L_{n+1\_r}}}, \quad n = 0, 1, 2, 3, \ldots, N-1. \tag{1}$$

Coupling coefficients between other coils can be neglected with a proper coil design as discussed in Section III.

A. System Modeling

The fundamental harmonics approximation (FHA) method is used to analyze the proposed WPT repeater system. Fig. 2 shows the equivalent circuit of the proposed WPT repeater system using the mutual inductance model. $\boldsymbol{I}_{0\_t}, \boldsymbol{I}_{1\_r}, \boldsymbol{I}_{1\_t}, \boldsymbol{I}_{2\_r}, \boldsymbol{I}_{2\_t}$, etc., are the currents flowing through $coil_{0\_t}$, $coil_{1\_r}$, $coil_{1\_t}$, $coil_{2\_r}$, $coil_{2\_t}$, etc., respectively, the directions of which are positive when the currents flow into the dot terminals of these coils. In practical applications, the "Driver" block in Fig. 1 is a rectifier circuit to transform the ac source to dc source because the dc power supply is needed for the driver circuit. Usually, the load can be regarded as resistive because the current and voltage on the rectifier are in the same phase. Thus, in the following context the "Driver" blocks are modeled as load resistors $(R_1, R_2, \ldots, R_N)$ to simplify the analysis. r_{0_t}, r_{1_r}, r_{1_t}, r_{2_r}, etc., are the equivalent parasitic resistances of the respective coils. ω_0 is the operational angular frequency of the system.

V_0 is the root mean square (RMS) value of the fundamental voltage component applied on the transmitting coil $coil_{0\_t}$. When the full bridge works in complementary manner, V_0 can be calculated using the dc link voltage $V_{\rm dc}$ as

$$V_0 = \frac{2\sqrt{2}}{\pi} V_{\rm dc}. \tag{2}$$

According to the Kirchhoff's voltage law, the voltage equations of the WPT repeater system can be written as

$$\begin{bmatrix} \boldsymbol{V}_0 \\ 0 \\ 0 \\ 0 \\ \ldots \\ 0 \end{bmatrix} = \begin{bmatrix} Z_{0\_t} & j\omega_0 M_{0\_1} & 0 & 0 & \ldots & 0 \\ j\omega_0 M_{0\_1} & Z_{1\_r} & j\omega_0 L_{f1} & 0 & \ldots & 0 \\ 0 & j\omega_0 L_{f1} & Z_{1\_t} & j\omega_0 M_{1\_2} & \ldots & 0 \\ 0 & 0 & j\omega_0 M_{1\_2} & Z_{2\_r} & \ldots & 0 \\ \ldots & \ldots & \ldots & \ldots & \ldots & \ldots \\ 0 & 0 & 0 & \ldots & \ldots & Z_{N\_r} \end{bmatrix} \cdot \begin{bmatrix} \boldsymbol{I}_{0\_t} \\ \boldsymbol{I}_{1\_r} \\ \boldsymbol{I}_{1\_t} \\ \boldsymbol{I}_{2\_r} \\ \ldots \\ \boldsymbol{I}_{N\_r} \end{bmatrix} \tag{3}$$

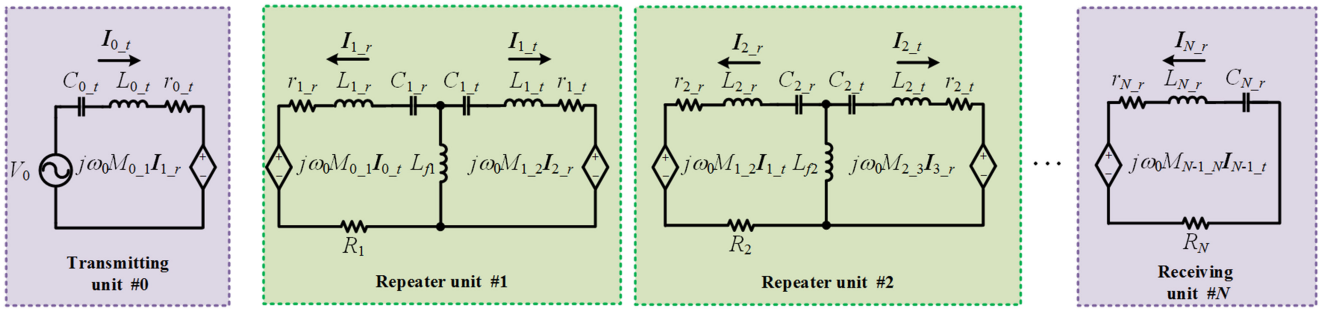

Fig. 2. Equivalent circuit of the proposed WPT repeater system using FHA method.

where $Z_{0\_t}=r_{0\_t}+j(\omega_0 L_{0\_t}-1/\omega_0 C_{0\_t})$, $Z_{1\_r}=R_1+r_{1\_r}+j(\omega_0 L_{1\_r}+\omega_0 L_{f1}-1/\omega_0 C_{1\_r})$, $Z_{1\_t}=r_{1\_t}+j(\omega_0 L_{1\_t}+\omega_0 L_{f1}-1/\omega_0 C_{1\_t})$, $Z_{2\_r}=R_2+r_{2\_r}+j(\omega_0 L_{2\_r}+\omega_0 L_{f2}-1/\omega_0 C_{2\_r})$, $\ldots$, $Z_{N\_r}=R_N+r_{N\_r}+j(\omega_0 L_{N\_r}-1/\omega_0 C_{N\_r})$.

B. Working Principle

In the proposed topology, the compensation capacitors and inductors are designed to satisfy the following conditions:

$$\omega_0 = 1/\sqrt{L_{0\_t}C_{0\_t}} = 1/\sqrt{(L_{1\_r}+L_{f1})C_{1\_r}} = 1/\sqrt{(L_{1\_t}+L_{f1})C_{1\_t}} = \cdots = 1/\sqrt{L_{N\_r}C_{N\_r}}. \quad (4)$$

The coil resistances are usually so small that can be neglected when analyzing the principle of the circuit. Substituting (4) into (3), the load currents can be calculated as

$$\begin{aligned} \boldsymbol{I}_{1\_r} &= \boldsymbol{V}_0/j\omega_0 M_{0\_1}, \quad \boldsymbol{I}_{2\_r} = -L_{f1}\boldsymbol{I}_{1\_r}/M_{1\_2}, \\ \boldsymbol{I}_{3\_r} &= -L_{f2}\boldsymbol{I}_{2\_r}/M_{2\_3}, \ldots, \\ \boldsymbol{I}_{N\_r} &= -L_{f(N-1)}\boldsymbol{I}_{N-1\_r}/M_{N-1\_N}. \end{aligned} \quad (5)$$

As can be seen from (5), once the system parameters such as the auxiliary inductances and mutual inductances are set, $\boldsymbol{I}_{1\_r}, \boldsymbol{I}_{2\_r}, \boldsymbol{I}_{3\_r}, \ldots, \boldsymbol{I}_{N\_r}$ are constant and independent of the load resistances. Since the loads are connected in series with $coil_{1\_r}, coil_{2\_r}, coil_{3\_r}, \ldots, coil_{N\_r}$, RMS values of the currents flowing through the loads remain constant regardless of the load variations. Moreover, RMS values of $\boldsymbol{I}_{1\_r}, \boldsymbol{I}_{2\_r}, \boldsymbol{I}_{3\_r}, \ldots, \boldsymbol{I}_{N\_r}$ are identical if the auxiliary inductances and mutual inductances meet the following equation:

$$L_{f1} = M_{1\_2}, \quad L_{f2} = M_{2\_3}, \ldots, \quad L_{f(N-1)} = M_{N-1\_N}. \quad (6)$$

Especially, all the inductances and mutual inductances can be designed with the same value, i.e.,

$$L_{f1}=L_{f2}=\cdots=L_{f(N-1)}=M_{1\_2}=\cdots=M_{N-1\_N}=M. \quad (7)$$

Therefore, equal power distribution among all the loads can be obtained with equal load resistances, i.e., $R_1 = R_2 = \cdots = R_N = R$. It can be seen that the charging conditions for all the loads are the same no matter how far the distance between each unit and the transmitter is.

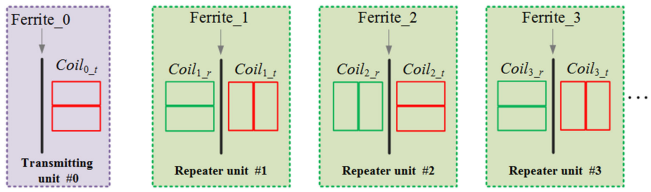

Fig. 3. Coil structure of the proposed WPT repeater system.

III. Coil Design

Based on the above analysis, coupling coefficients between nonadjacent coils and the two coils in the same repeater unit should be as low as possible in order to obtain the load-independent constant current characteristics for the proposed WPT repeater system.

A. Coil Structure

The two coils in the same repeater unit are placed close to each other to realize a compact design. However, the coupling coefficient between these two coils is not desirable in the proposed WPT repeater system as explained above. In this paper, bipolar coils [23], [24] are adopted in the proposed system as shown in Fig. 3. In the same repeater unit, the two bipolar coils are perpendicularly placed so their coupling coefficient can be eliminated [24]. Ferrite plates are inserted not only between the two coils in the same repeater unit but also beside the transmitting and receiving coils to increase the coupling effects between the adjacent units. The two coils between the two adjacent ferrites, such as $coil_{0\_t}$ and $coil_{1\_r}$, are totally the same, so that enough coupling coefficients between these two coils can be obtained.

B. Finite Element Analysis (FEA)

The three-dimensional FEA simulation using MAXWELL has been conducted to design the coils as shown in Fig. 4. According to the application requirement, the distance between the two adjacent units is $d = 60$ mm. The side length of the coils is chosen as $l_{\text{coil}} = 160$ mm to obtain enough coupling. Then the width of the coils l_w and the side length of the ferrite plates l_{fe} need to be determined. Fig. 5 shows the variation of the coupling coefficient between adjacent repeater units with different l_w and l_{fe} using MAXWELL. When l_w increases from 10 to

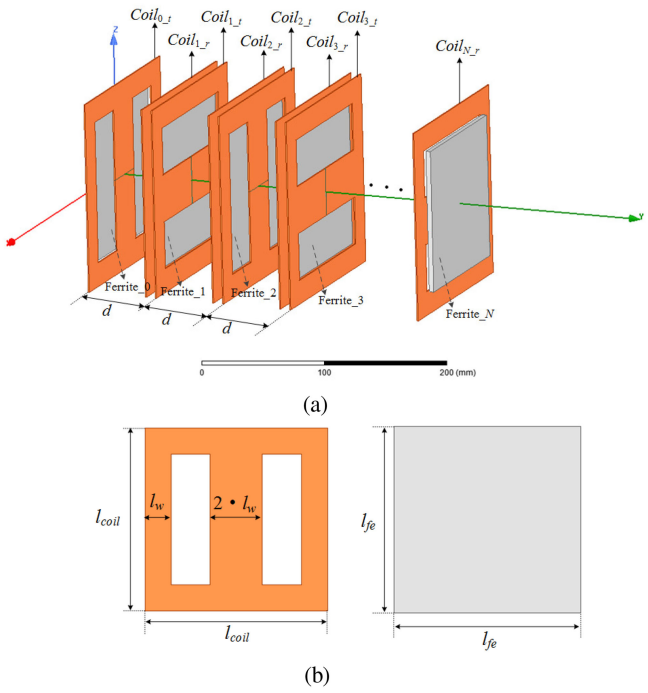

Fig. 4. FEA simulation model of the proposed WPT repeater system. (a) FEA simulation model. (b) Coil and ferrite dimensions.

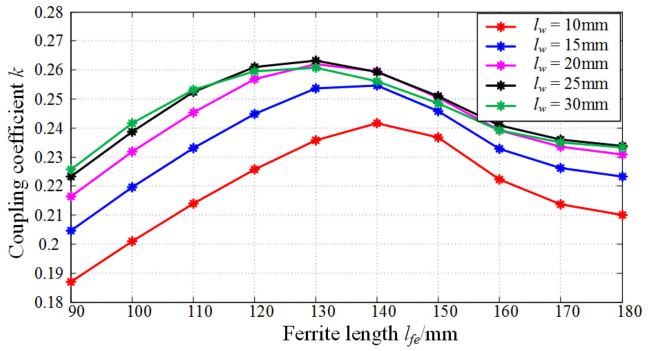

Fig. 5. Variation of the coupling coefficient between adjacent repeater units with different l_w and l_{fe}.

25 mm, the coupling coefficient k also increases. However, if l_w increases further, k begins to decrease. Thus, l_w is chosen as 20 mm in this case. Moreover, when l_{fe} increases, the coupling coefficient k first increases then decreases. The coupling coefficient k maintains at a relatively high value when l_{fe} varies between 100 and 140 mm. So l_{fe} is selected as 120 mm.

k_{1r_1t}, k_{1r_2r}, k_{1r_2t}, k_{1_2} are defined as the coupling coefficient between $coil_{1\_r}$ and $coil_{1\_t}$, $coil_{1\_r}$ and $coil_{2\_r}$, $coil_{1\_r}$ and $coil_{2\_t}$, $coil_{1\_t}$ and $coil_{2\_r}$. Because of the symmetric characteristics, these four coupling coefficients are sufficient to characterize the system. Table I compares the coupling coefficients of the proposed coil design with and without the ferrite plates. When there are no ferrite plates in the system, k_{1_2} is only 0.1190, which is smaller than the coupling coefficient of 0.2568 when the ferrite plates exist. k_{1r_1t} and k_{1r_2r} are always very small regardless of the existence of ferrites. That is because $coil_{1\_r}$ and $coil_{1\_t}$ or $coil_{2\_r}$ are placed perpendicularly. Moreover, k_{1r_2t} is

TABLE I
COUPLING COEFFICIENTS FOR THE PROPOSED COIL DESIGN

Ferrite dimension	No ferrite	120mm*120mm
k_{1r_1t}	0.000582	0.0001
k_{1r_2r}	0.000034	0.000108
k_{1r_2t}	0.06515	0.006395
k_{1_2}	0.1190	0.2568

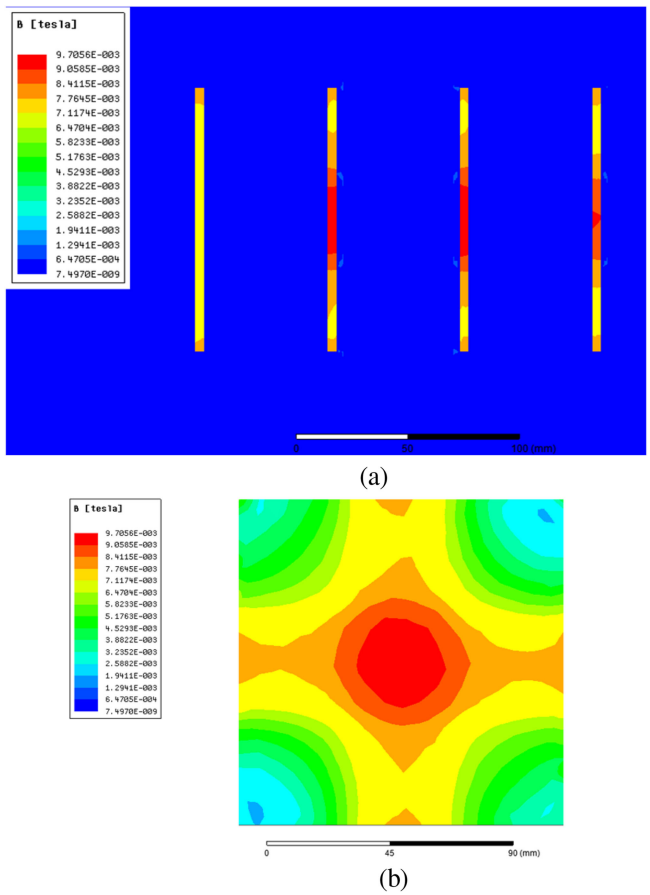

Fig. 6. Magnetic field distribution of the proposed WPT system. (a) Magnetic field in the *YZ* plane. (b) Magnetic field in Ferrite_1.

0.06515 when there is no ferrite, which brings cross-coupling to the system especially when the repeater unit number increases, and the cross-coupling effects will be superimposed. When using ferrite plates, k_{1r_2t} can be decreased to 0.006395, which is much smaller than k_{1_2}, so it can be neglected. Therefore, the ferrite plates not only increase the coupling between the adjacent units and increase the power transfer capability, but also provide magnetic insulations between the nonadjacent coils. Thus, only the coupling effect between $coil_{1\_t}$ and $coil_{2\_r}$ needs to be considered.

Fig. 6 shows the magnetic field distribution in the proposed WPT system. Because of the symmetrical characteristics of the coils, only three repeater units (#1, #2, and #3) and the transmitting unit are simulated. The magnetic field is mainly restricted in the ferrite plates and the magnetic field emission in the air is

very small. Fig. 6(b) shows the magnetic field in Ferrite_1. The largest magnetic flux density B lies in the center of the ferrite plate, which is about 9.84 mT.

IV. Power Transfer Capability

A. Influence of Parasitic Resistances

In a practical system, parasitic resistances of the coils are inevitable and their influence on the system needs to be analyzed. The quality factors of $coil_{0\_t}$, $coil_{1\_r}$, $coil_{1\_t}, \ldots, coil_{N\_r}$ are defined as Q_{0_t}, Q_{1_r}, $Q_{1\_t}, \ldots, Q_{N\_r}$, respectively. Then the parasitic resistances can be expressed using the quality factor as

$$r_i = \omega_0 L_i / Q_i \tag{8}$$

where the subscript i indicates the coil number. The reflected impedances in the coils can be calculated as

$$\begin{cases} Z_{r,N\_r} = 0 \\ Z_{r,n\_t} = \frac{(\omega_0 M_{n\_n+1})^2}{r_{n+1\_r} + R_{n+1} + Z_{r,n+1\_r}}, & n = 0, 1, 2, \ldots, N-1 \\ Z_{r,n\_r} = \frac{(\omega_0 L_{fn})^2}{r_{n\_t} + Z_{r,n\_t}}, & n = 1, 2, 3, \ldots, N-1. \end{cases} \tag{9}$$

Then the currents flowing through the coils can be calculated using the reflected impedances as

$$\begin{cases} \boldsymbol{I}_{0\_t} = \frac{\boldsymbol{V}_0}{r_{0\_t} + Z_{r,0\_t}} \\ \boldsymbol{I}_{n\_r} = -\frac{j\omega_0 M_{n-1\_n} \boldsymbol{I}_{n-1\_t}}{r_{n\_r} + R_n + Z_{r,n\_r}}, & n = 1, 2, 3, \ldots, N \\ \boldsymbol{I}_{n\_t} = -\frac{j\omega_0 L_{fn} \boldsymbol{I}_{n\_r}}{r_{n\_t} + Z_{r,n\_t}}, & n = 1, 2, 3, \ldots, N-1. \end{cases} \tag{10}$$

Since all these coils are the same, their quality factors are identical, i.e., $Q_{0\_t} = Q_{1\_r} = Q_{1\_t} = \cdots = Q_{N\_r} = Q$. The coupling coefficient between any two adjacent repeater units are also the same, i.e., $k_{0\_1} = k_{1\_2} = k_{2\_3} = \cdots = k_{N-1\_N} = k$. As discussed in Section II, (7) should be met in order to obtain identical RMS values of all the load currents. Now considering the parasitic resistances, the load currents can be calculated based on (10) and the results are shown in Fig. 7 where $N = 10$, $k = 0.1$, and $Q = 500$. The ten load resistances are identical and vary simultaneously. In order to facilitate comparisons, normalized load resistances and currents are used with their base values defined as

$$R_b = \omega_0 M, I_b = V_0 / R_b. \tag{11}$$

As can be seen from Fig. 7(a), when the load resistances increase, the load currents decrease gradually. For example, the normalized value of I_{1_r} decreases from 0.962 with the normalized load resistance of 0.2 to 0.896 when the normalized load resistance increases to 0.8. Moreover, the load currents attenuate as the transmitting distance increases as shown in Fig. 7(b). The normalized load currents of I_{10_r} is 0.799 when the normalized load resistance is 0.2, which is 83.1% of I_{1_r}. The load current attenuation rates depend on the load resistance. As the load resistances increase, the current attenuation rates become larger. When the normalized load resistance is 0.8, the normalized load current I_{10_r} decreases to 0.490, which is only 54.7% of I_{1_r}.

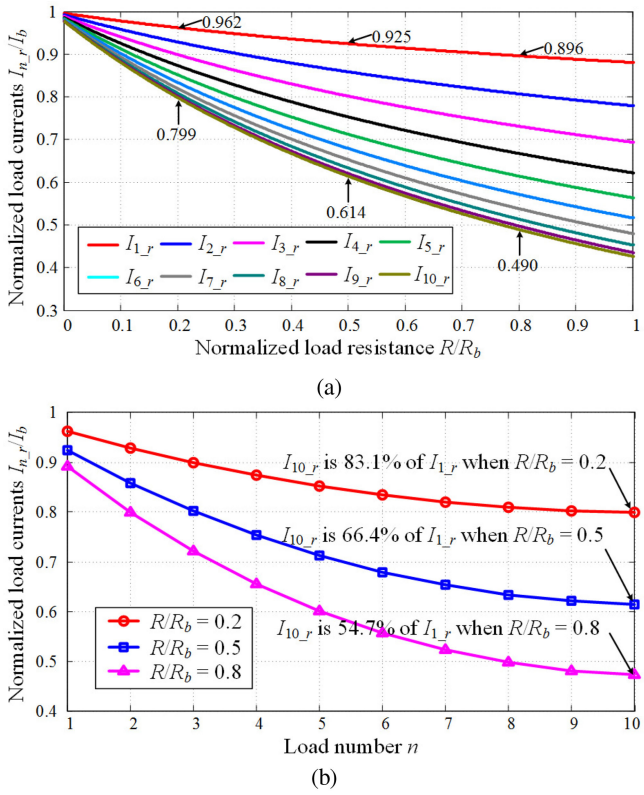

Fig. 7. Load current characteristics along with the load resistance variations ($k = 0.1$, $Q = 500$). (a) Load currents variation with load resistances. (b) Load current variations in different repeater units.

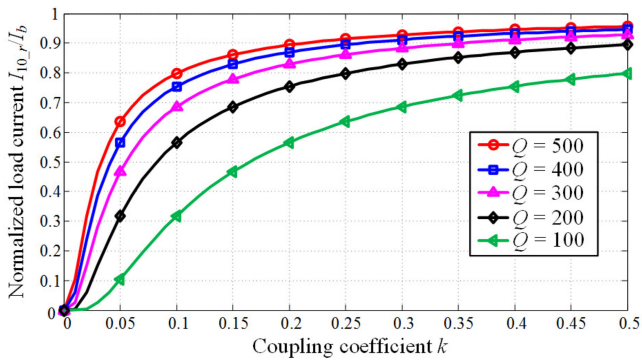

Fig. 8. Load current variations with different coupling coefficients and quality factors ($N = 10$, $R/R_b = 0.2$).

Fig. 8 shows the current variation flowing through the 10th load with different coupling coefficients and quality factors when $N = 10$ and $R/R_b = 0.2$. As the coupling coefficient k increases, the load current also increases. Moreover, a larger quality factor Q leads to a higher load current. It means that the load current attenuation rate can be decreased with a higher k and Q. Thus, a higher k and Q are beneficial from the perspective of constant load current outputs.

B. System Efficiency

The efficiency of each power unit is defined as $\eta_n (n = 1, 2, \ldots, N)$ where there are totally N loads. The efficiency of the whole system is defined as η. It can be found that $\eta = \eta_1$.

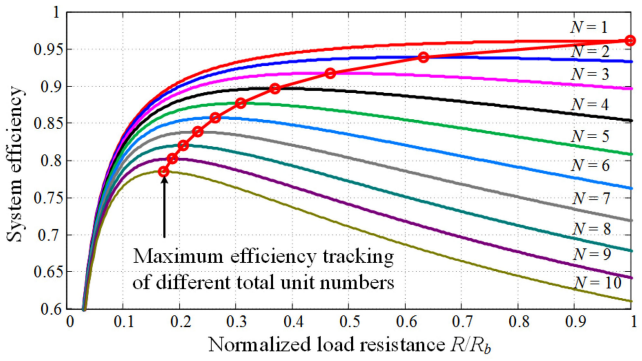

Fig. 9. System efficiency variations at different load resistances ($k = 0.1$, $Q = 500$).

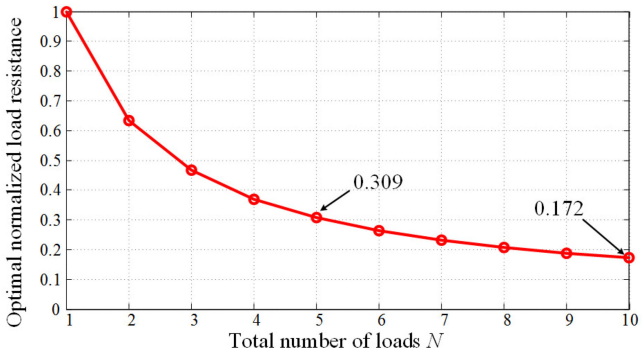

Fig. 10. Optimal load resistances to achieve maximum system efficiency with different number of loads ($k = 0.1$, $Q = 500$).

The efficiency can be calculated as

$$\eta_n = \frac{Z_{r,(n-1)t}}{r + Z_{r,(n-1)t}} \cdot \frac{R}{r + R + Z_{r,nr}} + \frac{Z_{r,(n-1)t}}{r + Z_{r,(n-1)t}} \cdot \frac{Z_{r,nr}}{r + R + Z_{r,nr}} \cdot \eta_{(n+1)}, \quad n = 1, 2, \ldots, N-1. \tag{12}$$

For the last load, the efficiency η_N can be calculated as

$$\eta_N = \frac{Z_{r,(N-1)t}}{r + Z_{r,(N-1)t}} \cdot \frac{R}{r + R} = \frac{Q_L \cdot (kQ)^2}{(1 + Q_L)^2 + (1 + Q_L)(kQ)^2} \tag{13}$$

where $Q_L = R/r$.

Based on (12) and (13), the system efficiency variations against the normalized load resistance are shown in Fig. 9 assuming that all the load resistances are identical. When $N = 1$, which is the traditional two-coil WPT system, the maximum efficiency is achieved when the normalized load resistance is about 1 and depends only on the coupling coefficient k and quality factor Q as reported in [2]. The optimal load resistance to achieve maximum system efficiency decreases as the repeater number increases as shown in Figs. 9 and 10. When N increases to 5, the optimal normalized load resistance decrease to 0.309 ($k = 0.1$, $Q = 500$). The number decreases to 0.172 when $N = 10$.

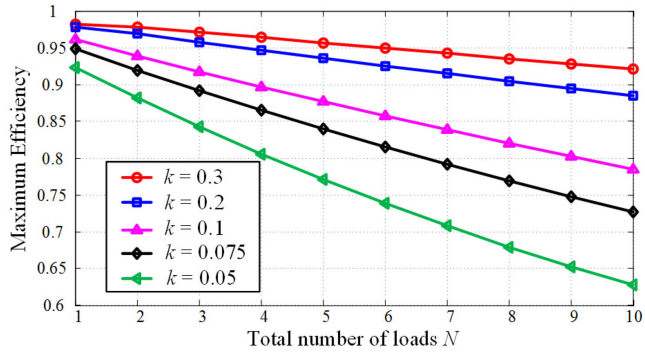

Fig. 11. Maximum achievable efficiency with different number of loads ($Q = 500$).

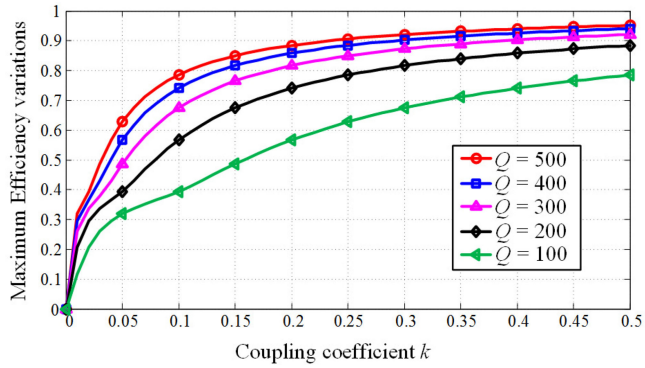

Fig. 12. Maximum achievable efficiency variations with coupling coefficient k and quality factor Q ($N = 10$).

Moreover, with the increasing of load number N, the maximum achievable system efficiency declines as shown in Fig. 11. This is because more power is consumed by the coil parasitic resistances. This figure provides some guidelines for system designs. For example, when the coupling coefficient $k = 0.1$ and quality factor $Q = 500$, the maximum load number should not exceed 10 if the efficiency is required to be above 0.8.

Fig. 12 shows the variations of the maximum achievable efficiency along with the coupling coefficient k and quality factor Q. Similar to the two-coil WPT system, the maximum achievable efficiency increases as k or Q increases. To transfer power via a long distance with a satisfactory system efficiency, a larger k or Q is preferred.

V. Experimental Results

A. System Design Procedure

In order to design the specific constant load current, the mutual inductance $M_{n\_n+1}(n = 0, 1, 2, \ldots, N-1)$ can be calculated based on (5). Then, the dimension of the coils can be determined with a given load distance with the help of MAXWELL. After making the coils, the self-inductances $L_{i\_t}(i = 0, 1, 2, \ldots, N-1)$, $L_{j\_r}(j = 1, 2, 3, \ldots, N)$, and mutual inductances $M_{n\_n+1}(n = 0, 1, 2, \ldots, N-1)$ of the coils can be measured. Based on (6), the auxiliary inductances $L_{fn}(n = 1, 2, 3, \ldots, N)$ can be obtained, which should be equal to the mutual inductances $M_{n\_n+1}(n = 0, 1, 2, \ldots,$

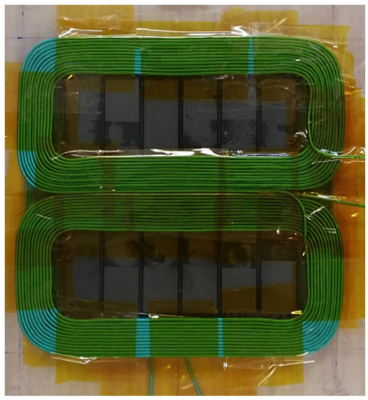

(a)

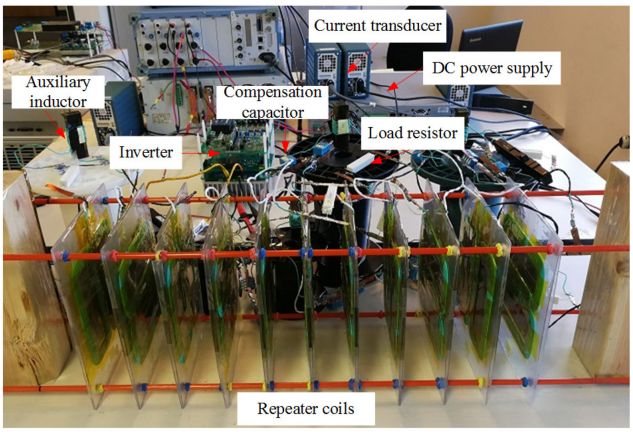

(b)

Fig. 13. Experimental setup of the proposed WPT system. (a) Repeater unit. (b) Experimental platform.

$N-1$). With the self-inductances $L_{i\_t}(i=0,1,2,\ldots,N-1)$ and the mutual inductances $M_{n\_n+1}(n=0,1,2,\ldots,N-1)$, the compensation capacitances $C_{i\_t}(i=0,1,\ldots,N-1)$ and $C_{j\_r}(j=1,2,\ldots,N)$ can be calculated using (4).

B. Experimental Setup

The experimental setup of the proposed WPT repeater system with ten loads has been constructed as shown in Fig. 13. The coils are made of the 660-strand Litz wires so that the skin effect can be neglected, which are installed on the plexiglass plates. The ferrite plates (PC40) are used in every unit. The dimension of the coils is 160 mm $\times$ 160 mm and that of the ferrite plate is 120 mm $\times$ 120 mm with the thickness of 4 mm. The turn number of the coil is 12. Four plastic rods pass through all the repeater units to fix the coils. The inverter consisting of four silicon carbide MOSFETs (C2M0080120D) is used to generate a 200 kHz ac voltage for the transmitting coil. The distance between adjacent units is fixed to 60 mm.

The self-inductances of the coils are measured around 93 μH. The coupling coefficient of the two adjacent coils in the two adjacent units (k_{0_1}, k_{1_2}, k_{2_3}, ...) is around 0.24, which is basically consistent to the simulation result in Section III. The auxiliary inductances are designed as 23 μH so that identical load currents can be obtained as shown in (7). The quality factor of the resonant loop is about 280. All the circuit parameters are listed in Table II.

TABLE II
CIRCUIT PARAMETERS OF THE EXPERIMENTAL SETUP

Parameter	Value	Parameter	Value
V_{dc}	30 V	f_s	200 kHz
l_{coil}	160 mm	l_{fe}	120 mm
l_w	20 mm	d	60 mm
$L_{0\_t} \sim L_{10\_r}$	93 μH	Q	280
$C_{1\_r} \sim C_{9\_t}$	5.46 nF	k	0.24
C_{0_t}, C_{10_r}	6.81 nF	$L_{f1} \sim L_{f9}$	23 μH

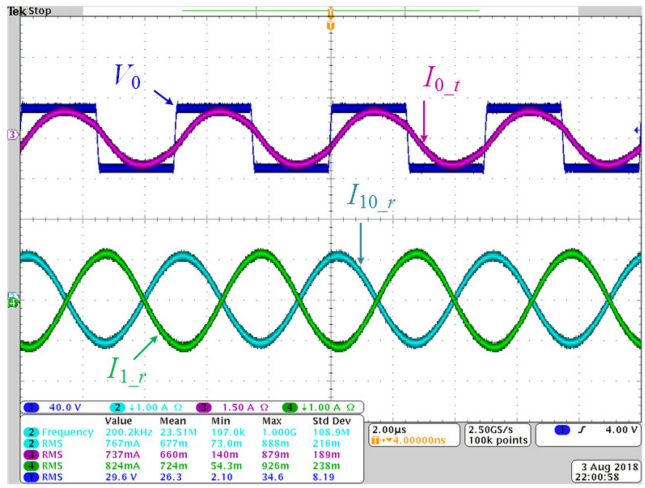

Fig. 14. Experimental waveforms of the voltages and currents.

In FACTS, the power electronics switches are usually identical and use a modular design. Thus, the driver circuits for these switches are identical and can be placed with the same distance. In the proposed WPT system, all the coils are identical and placed with the same distance to meet the requirements in such an application. Once the system is set, the distance between adjacent units will not change. It needs to be pointed out that the coupling coefficients or the quality factors are nearly identical although there exists installation errors in a practical implementation.

C. Experimental Results

A dc source is used to provide the dc-link voltage of 30 V for the experimental system. In the proposed WPT experimental setup, the output current is about 0.8 A and the total load power is about 25 W at the maximum system efficiency. When the dc voltage becomes larger, the load current and the load power will also increase. The experimental waveforms are shown in Fig. 14. It can be seen that the current $\boldsymbol{I}_{0\_t}$ slightly lags behind the input voltage $\boldsymbol{V}_0$ to achieve zero-voltage-switching (ZVS) for the MOSFETs so that the switching loss can be reduced. The first load current $\boldsymbol{I}_{1\_r}$ lags behind $\boldsymbol{I}_{0\_t}$ by about 90° and the 10th load current $\boldsymbol{I}_{10\_r}$ lags behind $\boldsymbol{I}_{1\_r}$ by about 180° as analyzed above.

The oscilloscope only has four channels and the ten load currents cannot be captured simultaneously in the same figure. Thus, the load currents when the load resistance is 3 Ω are captured using the oscilloscope and redrawn using MATLAB

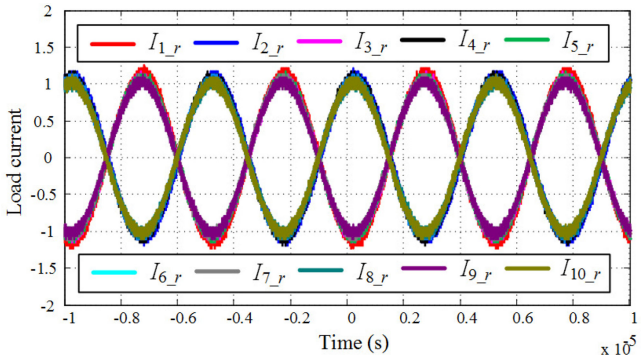

Fig. 15. Waveforms of the ten load currents.

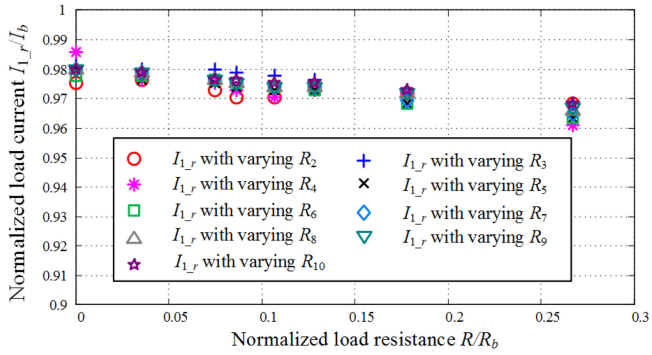

Fig. 17. Normalized I_{1_r} against the variation of other load resistances.

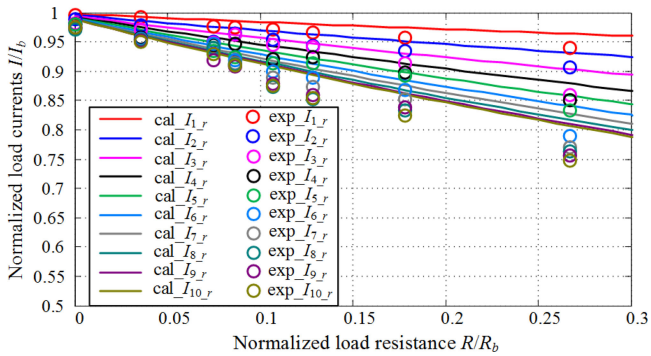

Fig. 16. Comparisons between calculated and experimental load currents ($k = 0.24$, $Q = 280$).

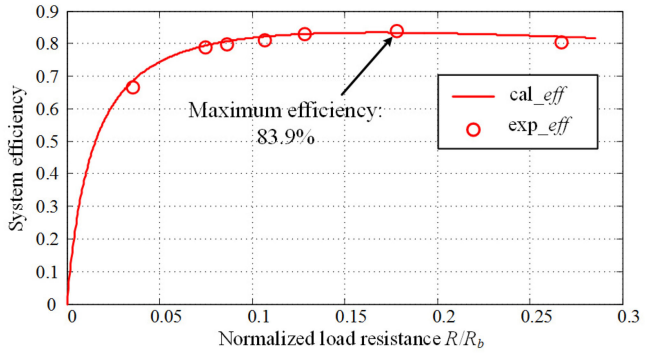

Fig. 18. Comparisons between calculated and experimental system efficiency ($k = 0.24$, $Q = 280$).

as shown in Fig. 15. The amplitudes of these currents are nearly the same.

The output currents flowing through the ten loads with various load resistances are normalized and shown in Fig. 16. The solid lines are the calculated load currents while the dots are the experimental results. All the currents and load resistance are normalized by dividing the base values of the currents and resistance shown in (11). As the load resistance increases, the load current gradually decreases because of the coil's parasitic resistance. The maximum load current drop of I_{10_r} is nearly 25% when the normalized load resistance about 0.27. Considering that there are ten loads in the experimental system, such current variation is acceptable. The experimental current is a little smaller than the calculated value. That is because the voltage drop on the reactance in $coil_{0\_t}$ increases when the load power increases to obtain ZVS. Thus, V_0 and the load current will decrease a little.

The load current I_{1_r} against the variations of other load resistances is shown in Fig. 17 as an instance. In each case only one load resistance is changed. For example, the other normalized load resistances remain constant as 0.17 when R_2 is varying. It can be seen from Fig. 17 that I_{1_r} slightly decreases when the other load resistance increases and the variation is within 2%. Thus, the load current and power of a repeater is basically unaffected by other loads.

Fig. 18 shows the system efficiency variations against the load resistance. It can be seen from Fig. 18 that the measured system efficiency matches the calculated efficiency well. The maximum efficiency is measured as 83.9% when the normalized load resistance is around 0.17 ($k = 0.24$, $Q = 280$). When the coupling coefficient k or quality factor Q becomes larger, the reachable maximum efficiency can be higher.

VI. Conclusion

In this paper, a novel WPT system has been proposed, which can power multiple loads simultaneously by using repeater coils. Such a system can be used for the driver circuits in FACTS where the repeater unit not only transfers power to the next unit, but also provides power to the driver circuits connected to them. Two bipolar coils placed perpendicularly together with ferrite inserted between them are used in every repeater unit. With the proposed compensation circuits, the system ensures constant load currents regardless of the load variations. As a result, independent load power control can be realized. The load current characteristics and system efficiency have been analyzed when considering the coil parasitic resistances. It was shown that a higher coupling coefficient k and quality factor Q is beneficial to maintain constant load current characteristics and improve the system efficiency. Experimental results have validated the effectiveness of the proposed WPT repeater system.

References

[1] Z. Zhang, H. Pang, A. Georgiadis, and C. Cecati, "Wireless power transfer—An overview," *IEEE Trans. Ind. Electron.*, vol. 66, no. 2, pp. 1044–1058, Feb. 2019.

[2] S. Li and C. C. Mi, "Wireless power transfer for electric vehicle applications," *IEEE J. Emerg. Sel. Topics Power Electron.*, vol. 3, no. 1, pp. 4–17, Mar. 2015.

[3] Q. Zhu, Y. Zhang, C. Liao, Y. Guo, L. Wang, and F. Li, "Experimental study on asymmetric wireless power transfer system for electric vehicle considering ferrous chassis," *IEEE Trans. Transp. Electrific.*, vol. 3, no. 2, pp. 427–433, Jun. 2017.
[4] C. Xiao, D. Cheng, and K. Wei, "An LCC-C compensated wireless charging system for implantable cardiac pacemakers: Theory, experiment, and safety evaluation," *IEEE Trans. Power Electron.*, vol. 33, no. 6, pp. 4894–4905, Jun. 2018.
[5] J. Yin, D. Lin, C. K. Lee, T. Parisini, and S. Y. R. Hui, "Front-end monitoring of multiple loads in wireless power transfer systems without wireless communication systems," *IEEE Trans. Power Electron.*, vol. 31, no. 3, pp. 2510–2517, Mar. 2016.
[6] S. Y. R. Hui, "Past, present and future trends of non-radiative wireless power transfer," *CPSS Trans. Power Electron. Appl.*, vol. 1, no. 1, pp. 83–91, Dec. 2016.
[7] D. Ahn and S. Hong, "A study on magnetic field repeater in wireless power transfer," *IEEE Trans. Ind. Electron.*, vol. 60, no. 1, pp. 360–371, Jan. 2013.
[8] S. Y. R. Hui, W. X. Zhong, and C. K. Lee, "A critical review of recent progress in mid-range wireless power transfer," *IEEE Trans. Power Electron.*, vol. 29, no. 9, pp. 4500–4511, Sep. 2014.
[9] W. X. Zhong, C. K. Lee, and S. Y. R. Hui, "Wireless power domino-resonator systems with noncoaxial axes and circular structures," *IEEE Trans. Power Electron.*, vol. 27, no. 11, pp. 4750–4762, Nov. 2012.
[10] C. K. Lee, W. X. Zhong, and S. Y. R. Hui, "Effects of magnetic coupling of nonadjacent resonators on wireless power domino-resonator systems," *IEEE Trans. Power Electron.*, vol. 27, no. 4, pp. 1905–1916, Apr. 2012.
[11] K. Lee and S. H. Chae, "Power transfer efficiency analysis of intermediate-resonator for wireless power transfer," *IEEE Trans. Power Electron.*, vol. 33, no. 3, pp. 2484–2493, Mar. 2018.
[12] J. Lee, K. Lee, and D. H. Cho, "Stability improvement of transmission efficiency based on a relay resonator in a wireless power transfer system," *IEEE Trans. Power Electron.*, vol. 32, no. 5, pp. 3297–3300, May 2017.
[13] M. Chabalko, J. Besnoff, M. Laifenfeld, and D. S. Ricketts, "Resonantly coupled wireless power transfer for non-stationary loads with application in automotive environments," *IEEE Trans. Ind. Electron.*, vol. 64, no. 1, pp. 91–103, Jan. 2017.
[14] P. K. S. Jayathurathnage, A. Alphones, and D. M. Vilathgamuwa, "Optimization of a wireless power transfer system with a repeater against load variations," *IEEE Trans. Ind. Electron.*, vol. 64, no. 10, pp. 7800–7809, Oct. 2017.
[15] C. Zhang, D. Lin, N. Tang, and S. Y. R. Hui, "A novel electric insulation string structure with high-voltage insulation and wireless power transfer capabilities," *IEEE Trans. Power Electron.*, vol. 33, no. 1, pp. 87–96, Jan. 2018.
[16] D. Karwatzki and A. Mertens, "Generalized control approach for a class of modular multilevel converter topologies," *IEEE Trans. Power Electron.*, vol. 33, no. 4, pp. 2888–2900, Apr. 2018.
[17] J. Chivite-Zabalza, P. Izurza-Moreno, D. Madariaga, G. Calvo, and M. A. Rodriguez, "Voltage balancing control in 3-level neutral-point clamped inverters using triangular carrier PWM modulation for FACTS applications," *IEEE Trans. Power Electron.*, vol. 28, no. 10, pp. 4473–4484, Oct. 2018.
[18] K. Kusaka, K. Orikawa, J. Itoh, K. Morita, and K. Hirao, "Isolation system with wireless power transfer for multiple gate driver supplies of a medium voltage inverter," in *Proc. Int. Power Electron. Conf.*, May 2014, pp. 191–198.
[19] Y. Zhang, T. Lu, Z. Zhao, K. Chen, F. He, and L. Yuan, "Wireless power transfer to multiple loads over various distances using relay resonators," *IEEE Microw. Wireless Compon. Lett.*, vol. 25, no. 5, pp. 337–339, May 2015.
[20] V. B. Vu, D. H. Tran, and W. Choi, "Implementation of the constant current and constant voltage charge of inductive power transfer systems with the doubled-sided LCC compensation topology for electric vehicle battery charge applications," *IEEE Trans. Power Electron.*, vol. 33, no. 9, pp. 7398–7410, Sep. 2018.
[21] W. Zhang, S. C. Wong, C. K. Tse, and Q. Chen, "Load-independent duality of current and voltage outputs of a series- or parallel-compensated inductive power transfer converter with optimized efficiency," *IEEE J. Emerg. Sel. Topics Power Electron.*, vol. 3, no. 1, pp. 137–146, Mar. 2015.
[22] J. Hou, Q. Chen, Z. Zhang, S. C. Wong, and C. K. Tse, "Analysis of output current characteristics for higher order primary compensation in inductive power transfer systems," *IEEE Trans. Power Electron.*, vol. 33, no. 8, pp. 6807–6821, Aug. 2018.
[23] M. Budhia, J. T. Boys, G. A. Covic, and C. Y. Huang, "Development of a single-sided flux magnetic coupler for electric vehicle IPT charging systems," *IEEE Trans. Ind. Electron.*, vol. 60, no. 1, pp. 318–328, Jan. 2013.
[24] T. Kan, F. Lu, T. D. Nguyen, P. P. Mercier, and C. C. Mi, "Integrated coil design for EV wireless charging systems using LCC compensation topology," *IEEE Trans. Power Electron.*, vol. 33, no. 11, pp. 9231–9241, Nov. 2018.

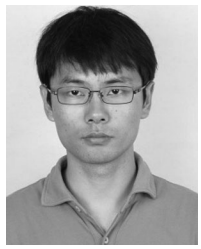

Chenwen Cheng received the B.S. and Ph.D. degree from Zhejiang University, Hangzhou, China, in 2012 and 2017, respectively, all in electrical engineering.

He is currently a Postdoc Researcher with San Diego State University, San Diego, CA, USA. His research interests include the motor control, renewable power generation, and wireless power transfer technologies.

Fei Lu (S'12–M'17) received the B.S. and M.S. degree from the Harbin Institute of Technology, Harbin, China, in 2010 and 2012, respectively, and the Ph.D. degree from the University of Michigan, Ann Arbor, MI, USA, in 2017, all in electrical engineering.

He is currently an Assistant Professor with the Department of Electrical and Computer Engineering, Drexel University, Philadelphia, PA, USA. His research topic focuses on power electronics and the application of electric vehicle charging.

Zhe Zhou received the B.E. degree in measure and control technology and instrumentations from the Changchun University of Science and Technology, Changchun, China, in 2011 and the M.S degree in power electronics and power drives from Tianjin University, Tianjin, China, in 2014.

He is currently with the State Key Laboratory of Advanced Power Transmission Technology (Global Energy Interconnection Research Institute), Beijing, China. His research interests include the applications of the wide-gap device and the solid state transformer.

Weiguo Li (M'01) received the B.S. degree from Northeast Dianli University, Jilin, China, in 1996, the M.S. degree from China Electric Power Research Institute, Beijing, China, in 2006, and Ph.D. degree from North China Electric Power University, Beijing, China, in 2013, all in electrical engineering.

He is currently with the State Key Laboratory of Advanced Power Transmission Technology (Global Energy Interconnection Research Institute), Beijing, China. His research interests include the flexible ac transmission systems and power systems.

Chong Zhu (M'17) received the B.S. degree in electrical engineering from the China University of Mining and Technology, Xuzhou, China, in 2010 and the Ph.D. degree in electrical engineering from Zhejiang University, Hangzhou, China, in 2016.

He is currently a Postdoc Researcher with San Diego State University, San Diego, California, USA. His research interests include battery thermal management, ac/dc power conversion, and pulsewidth modulation techniques applied in EVs.

Hua Zhang (S'14–M'17) received B.S., M.S., and Ph.D. degrees in electrical engineering from Northwestern Polytechnical University, Xi'an, China, in 2011, 2014, and 2017, respectively.

From September 2014 to August 2015, she was a joint Ph.D. student founded by the China Scholarship Council with the University of Michigan, Dearborn, MI, USA. From September 2015, she started to work with San Diego State University. She is currently a Postdoctoral Research Associate with Drexel University, Philadelphia, PA, USA. Her research focuses on the charging technology of electric vehicles.

Zhanfeng Deng received the B.S. and M.S. degrees in welding technology and equipment from Jilin Polytechnical University, Changchun, China, in 1996 and the Ph.D. degree in electrical engineering from Tsinghua University, Beijing, China, in 2003.

He is currently with the State Key Laboratory of Advanced Power Transmission Technology (Global Energy Interconnection Research Institute), Beijing, China. His research interests include the flexible ac transmission systems and power systems.

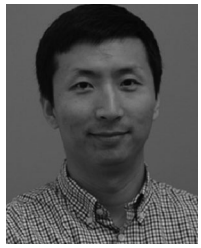

Xi Chen (S'07–M'13–SM'16) received the B.Eng. degree in information engineering from the Beijing Technology and Business University, Beijing, China, the M.Sc. degree in digital signal processing from Kings College London, University of London, London, U.K., and the Ph.D. degree in electronic and information engineering from the Hong Kong Polytechnic University, Hong Kong, in 2003, 2005, and 2009, respectively.

He was a Postdoctoral Research Fellow with the Institute of Software, Chinese Academy of Science, Beijing, China, from 2011 to 2013, and a Research Associate with the Hong Kong Polytechnic University, in 2009. He was a Visiting Student with the University of Florida, Gainesville, FL, USA, in 2008. In 2014, he joined GEIRI North America, San Jose, CA, USA, where he is currently the Chief Information Officer. From 2009 to 2014, he was with the Center of Internet of Things Research, the Department of Marketing, and the Scientific and Technological Achievements Award Center at State Grid Corporation of China, Beijing, China. His research interests include the Internet of Things, smart grids, electric vehicle charging infrastructure, and complex networks analysis and its applications.

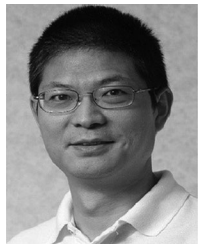

Chunting Chris Mi (S'00–A'01–M'01–SM'03–F'12) received the B.S.E.E. and M.S.E.E. degrees in electrical engineering from Northwestern Polytechnical University, Xi'an, China, and the Ph.D. degree in electrical engineering from the University of Toronto, Toronto, ON, Canada, in 1985, 1988, and 2001, respectively.

He is currently a Professor and the Chair of electrical and computer engineering and the Director of the Department of Energy-funded Graduate Automotive Technology Education Center for Electric Drive Transportation, San Diego State University (SDSU), San Diego, USA. Prior to joining SDSU, he was with University of Michigan, Dearborn, MI, USA, from 2001 to 2015.